

## Ionization cross sections of gases for protons at kinetic energies between 20 MeV and 385 GeV, and applications to vacuum gauges in superconducting accelerators

Hajime Ishimaru and Shinkichi Shibata\*

*National Laboratory for High Energy Physics (KEK), Tsukuba, Ibaraki-ken 305, Japan*

Mitio Inokuti

*Argonne National Laboratory, Argonne, Illinois 60439*

(Received 16 November 1994)

Measurements have been made of the ionization cross sections of air, hydrogen, and argon by use of the KEK 500-MeV booster, the KEK 12-GeV main ring, and the Fermilab main ring. Within the beam duct of each of those accelerators, we placed a gas ionization monitor and recorded the current in the monitor as a function of the time elapsed since the beam injection for each pulse. This time is uniquely related to the instantaneous kinetic energy of protons. Because gas pressure in the monitor was kept sufficiently low (about  $10^{-5}$  Torr), the current is attributable to single ionizing collisions of protons with molecules and is therefore proportional to the specific primary ionization, or the ionization cross section (rather than the total ionization). The dependence of the cross section on proton kinetic energy, measured for air, hydrogen, and argon, agrees closely with the prediction of the Bethe theory, and is represented by a straight line on the Fano plot. The data were tested for consistency with other measurements for electrons and protons at lower kinetic energies. Implications of the work for the design of accelerator vacuum components and of particle detectors are included. For instance, the technique used in the present measurements can be readily applied to the determination of the pressure distribution in a beam duct at liquid-helium temperature of an accelerator using superconducting magnets.

PACS number(s): 34.50.-s, 29.40.Cs, 29.20.Dh, 29.20.Lq

### I. INTRODUCTION

Cross sections for the ionization of gaseous molecules by high-energy protons are important in many applications, including particle physics, radiation physics, plasma physics, astrophysics, space research, and accelerator physics. Although measurements at proton energies up to several MeV have been reported for a number of gases, data are far from complete [1–3]. For protons at higher energies, only a few fragmentary data are available.

In several areas of accelerator physics, ionization cross-section data are required. Obvious examples include the design of a vacuum system of a synchrotron or a storage ring for electrons or protons and the development of high-energy particle detectors. In what follows, we discuss two specific applications in some detail.

The first application concerns measurements of gas pressure in a large-scale accelerator ring. It is now a standard practice to place a set of ionization vacuum gauges on the ring and thereby to determine the pressure distribution. A conventional ionization vacuum gauge that uses the ionization of a gas by electrons of about 150-eV kinetic energies is effective at sufficiently high pressures.

A storage ring, such as the LHC (Large Hadron Collider), for storing protons of ultrahigh energies will use

superconducting magnets and a beam tube cooled with liquid helium. In the event of leakage in the beam tube, the pressure rise will be local because of gas adsorption by nearby solid surfaces, which is especially efficient at liquid-helium temperatures [4]. Therefore, a vacuum gauge placed at some distance from the beam tube may fail to detect the pressure rise. Even though the pressure rise is local, it will affect the beam lifetime considerably. Thus, we may wish to set numerous vacuum gauges along the beam tube. However, no vacuum gauge operable at liquid-helium temperatures is available, and we would be obliged to set vacuum gauges at positions of room temperature; this arrangement would hardly detect the local pressure rise. A good solution of this problem would be to set ionization monitors within the beam tube to enable us to observe the local pressure rise.

At extremely low pressures (i.e., in the “ultrahigh vacuum”), the use of an ionization vacuum gauge is problematic because its electron source is a hot filament, which may emit some atomic particles. In a cryogenic beam duct in particular, the presence of a heated filament is impermissible. Thus if one is forced to place an ionization gauge at a position distant from the cryogenic beam duct, one will not obtain the true pressure in the duct.

If the cross section  $\sigma$  for the ionization of the residual gas by the beam particles is known, one may simply use an ionization detector. Provided that the efficiency and the volume for ion collection are constant, the signal  $s$  is proportional to  $pI_p\sigma$ , where  $p$  is the pressure and  $I_p$  is the beam intensity. Thus, a measured distribution of  $s$  along the ring can readily be converted to the pressure distribu-

---

\*Present address: Tsukuba College of Technology, Kasuga 4-12-7, Tsukuba, Ibaraki-ken 305, Japan.

tion. For this purpose, relative values of  $\sigma$  at different particle energies  $T$  are sufficient; one only needs to calibrate the pressure determination at a single position in the ring.

The second application concerns measurements of the beam intensity and position in a proton storage ring. A conventional beam monitor is subject to the influence of beam bunching and debunching. This influence is absent in an ionization detector. If  $\sigma$  is known, and if the pressure, efficiency, and volume of ion collection are constant, then the signal  $s$  can readily be converted to the beam intensity  $I_p$ .

During the design, operation, and beam monitoring of large-scale accelerators, we repeatedly felt the need for ionization cross sections, especially for the species present in the residual gas, such as air molecules. To meet the need, we used the principles of the work of DeLuca [5] and conducted a series of measurements that are greatly improved in accuracy, are more efficient in data processing, and cover a much wider range (20 MeV–385 GeV) of proton kinetic energy than DeLuca's earlier work. What follows is a comprehensive account of this effort, following up preliminary reports [6,7].

A basic theory for ionization and other energy-loss processes caused by fast charged particles was given by Bethe [8–10], and its consequences have been discussed from many points of view [11,12]. On theoretical grounds, cross sections for ionization by protons in our energy range should be well described by the Bethe theory. This expectation is also supported by empirical findings on electron collisions [13,14]. In particular, the Bethe theory predicts a definite analytic form for the energy dependence of the cross sections. This form contains two coefficients that are characteristic of the atom or molecule used as the target and are suitable objects of study in atomic and molecular physics. Therefore, we used elements of the Bethe theory to analyze our data.

## II. METHOD OF MEASUREMENTS

In a short, straight-line section of an accelerator, we placed an ionization detector and observed its output signal  $s$ , which is proportional to the ionization current that arises when we inject a gas into the detector. In another straight-line part, we placed a beam current monitor (i.e., a current transformer) to measure the proton beam current  $I_p$ . We kept the gas pressure and the collection efficiency of the ionization detector constant. Provided that the gas pressure is sufficiently low, the ionization arises from a single collision of a proton with a gaseous molecule, with no appreciable contribution by secondary electrons. Then, the ratio  $s/I_p$  is proportional to the ionization cross section  $\sigma$ .

A novelty of the present measurements is that the kinetic energy  $T$  of the protons is increasing continuously with time and that the relative value of  $\sigma$  is obtained as a function of  $T$ , even from a single period of acceleration. Good statistics on the measurements can be readily achieved by using repeated pulses. The measurement is nondestructive in the sense that it has no influence on the accelerator operation.

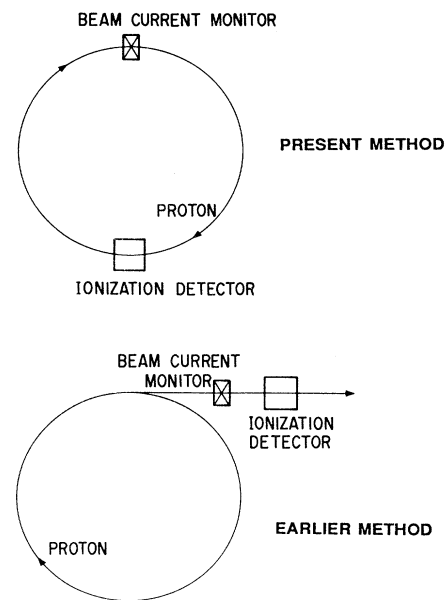


FIG. 1. Schematic diagrams comparing the present method of measurement (top) and the earlier standard method (bottom).

Figure 1 shows in schematic diagrams the contrast between earlier measurements and the present measurements. In earlier measurements, the proton beam was extracted from an accelerator and was led to an ionization chamber. To obtain protons of different kinetic energies, one had to extract the beam at different times. This often required cumbersome and time-consuming preparations.

## III. INSTRUMENTATION AND EXPERIMENTAL PROCEDURES

### A. Ionization detector

The ionization detector is an assembly of parallel plates made of stainless steel, as shown in Fig. 2. The plates act as electrodes when they are placed in the accelerator vacuum so that the proton beam passes between them. To achieve uniform intensity in the electric field between the plates, we used six dividing electrodes, connected

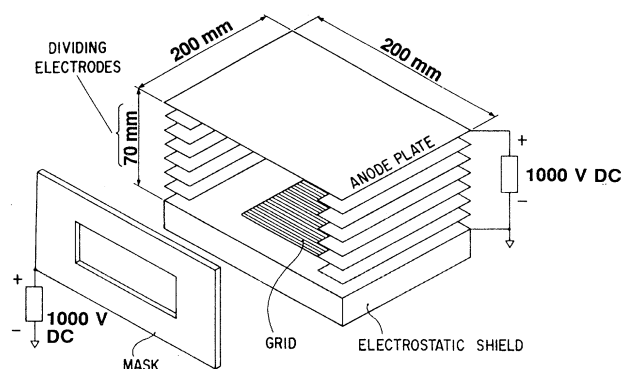


FIG. 2. Schematic view of the ionization detector.

through dividing resistors. As we increased the intensity of the electric field, the ion current increased and eventually became saturated at a value indicative of a full collection of ions. Saturation was achieved at an applied voltage of 1000 V. The size of the plates was  $200 \times 200 \text{ mm}^2$ , and the gap between them was 70 mm. The lower plate had a window of the size  $100 \times 100 \text{ mm}^2$ , over which a series of stainless steel wires of 0.08 mm diameter were placed at 2-mm intervals. This window size is sufficiently large to accommodate the closed-orbit distortion of the proton beam. At 10 mm below the wired grid, we placed another electrode for ion collection, also made of stainless steel,  $170 \times 120 \text{ mm}^2$  in size. The wired grid served as electrostatic shielding for the upper side of the ion collector and prevented electrostatically induced noise. For further electrostatic shielding, the outer and lower sides of the ion collector electrode were covered with thin films of stainless steel. We used alumina ceramics for electrical insulation of all the electrodes.

Some of the protons lost from the beam could have hit the inner surface of the vacuum beam duct and thereby generated unwanted secondary electrons. Secondary electrons that entered the ionization detector would cause noise in the signal and thus error in the measurement. To prevent this, we installed a mask for absorbing secondary electrons at a position upstream of the ionization detector. The design of the mask was based on measurements of secondary electrons produced by protons hitting tungsten wires deliberately placed in the beam chamber. The mask opening was chosen to be slightly smaller than the cross section of the beam chamber so that occasional stray protons would not affect the monitor. The mask was made from a 10-mm-thick stainless-steel plate. (We also installed another mask at a position downstream of the ionization detector, but we failed to observe any effect from it.)

### B. Gas injection

The normal equilibrium pressure in the beam duct of an accelerator is lower than  $10^{-7}$  Torr. For gas injection we used an automatic pressure controller built by Granville-Phillips Co. Each gas sample was stored in a reservoir tank that had been completely outgassed. We used an ion pump (with a pumping speed of 1 L/s) as a pressure gauge for the automatic controller and set an upper limit of gas injection at a pressure of  $10^{-5}$  Torr. (At an early stage of the work we used an ionization gauge for the same purpose; however, it was unstable and failed to give the feedback signals needed for pressure control.) The variation of the injected-gas pressure was kept below 1%.

### C. Efficiency of ion collection

Ions and electrons generated in the gas by the proton beam traveled 35 mm on the average before reaching an electrode. Collisions of ions and electrons with gas molecules were rare because the gas pressure was less than  $10^{-5}$  Torr. Indeed, the mean-free path between those collisions was about  $3 \times 10^3$  cm, much greater than the

distance of 6 cm between the ionization region and the ion collector. Thus, our measurements pertain to the primary ionization rather than the total ionization.

To substantiate the claim that  $s/I_p$  is proportional to  $\sigma$ , we must show that the efficiency of ion collection was constant (viz., independent of the proton kinetic energy). In general, the ions generated within the volume of the uniform electric field between the two electrodes were collected. To achieve full collection of the ions, we made the sizes of both the wire grid and the ion collector much larger than both the beam size and the closed-orbit distortion.

When the proton beam was sufficiently intense, the ions were generated so densely that space-charge effects may have driven some of the ions out of the collection volume; then, the efficiency of the ion collection would have been diminished. To test this possibility, we repeated measurements at widely varying beam intensities  $I_p$  with both the booster and the main ring at KEK. At  $I_p = 2 \times 10^{12}$  protons/pulse and with an applied voltage of 1000 V, the spread of the ionization region by space-charge effects was about 10%. The collector area was sufficiently large to cover this spread, as well as the beam size and the closed-orbit distortion. Consequently, we found that  $s/I_p$  was independent of  $I_p$ , indicating the constancy of ion collection efficiency in the range of  $I_p$  studied.

### D. Data acquisition and processing

The signal generated in the ionization detector went into an amplifier located next to it, traveled through a cable driver, and was eventually transmitted to a data processor in the control room. The amplifier was a model RCA 3140, of a field effect transistor input-operational type and having a gain of 20. The zero-level drift of the output signal was less than 5 mV (i.e., 0.5% of a typical output signal of about 1 V). Output signals from the ionization detector were fed to a transient recorder (Biomation 8100). Likewise, output signals from the beam current monitor were fed to another transient recorder. These two transient recorders were interfaced and connected with a minicomputer (Melcom-70) for processing the signals into output data, which were in turn displayed on a graphic terminal (Tektronix 4010).

We displayed the ionization cross section  $\sigma$  graphically as a function of the proton energy  $T$ . As for the vertical axis of such a graph, a relative value of  $\sigma$  was obtained readily as the ratio of the ionization signal  $s$  to the beam current  $I_p$ , as stated in the introduction. As for the horizontal axis,  $T$  was uniquely related to the time  $t$  since the beginning of the beam acceleration for each pulse. However, the functional relation between  $T$  and  $t$  is nonlinear in general and depends on the variation of the deflecting magnetic field with time. The strength of the deflecting magnetic field is simply related to the proton energy  $T$ . In the booster synchrotron of KEK (which accelerates protons from 20 to 500 MeV), the deflecting magnetic field is due to a magnet current that is represented by a sinusoidal shape with a bias. In the main ring of KEK, as well as that of Fermilab, the magnet current is

represented by a trapezoidal shape. We programmed a power supply so that it generated a clock pulse as output each time the strength of the deflecting magnetic field increased by  $10^{-5}$  T. We chose this frequency of the clock pulse to maximize the data sampling within the limit of the data volume allowable in a transient recorder. At the beginning and near the end of the magnetic-field rise, we registered every 110th clock pulse by using a counter, because the total number of clock pulses that could be stored in the recorder was limited to 1000; thus, we set the number of signal samples in the transient recorder at 970. We set the full scale for input to the recorder at 8 bits, so that the signal would not overscale.

It is useful to determine the position and the profile of the proton beam during measurements, to ensure that ions are completely collected. With this in mind, we designed the ion collector as follows. It consists of two triangular electrodes whose diagonals face each other, as seen in Fig. 3. If  $R^+$  and  $R^-$  represent output signals of the two electrodes, then the index

$$\Delta R = k(R^+ - R^-)/(R^+ + R^-) \quad (1)$$

represents the beam position,  $k$  being a constant. Thus, the ionization chamber also serves as a beam position detector.

Alternatively, we can use a multichannel collector for ion collection, as shown in Fig. 4. Then, we can obtain a beam profile from the output signals of the collector. Indeed, we have observed a beam profile, as seen in Fig. 5, by connecting a 32-channel collector to a sample-hold circuit.

To maximize the input signal and at the same time to avoid signal saturation, we adjusted a signal attenuator and thus accomplished a signal precision better than 10%. A single point in the detector system, including the amplifier and high-voltage supply, was grounded to prevent noise due to induction. The grounded part of the detector system and that of the data processing system were connected, but they were kept electrically separated by a 2-MHz analog photoisolator that prevented noise due to current in the ground loop.

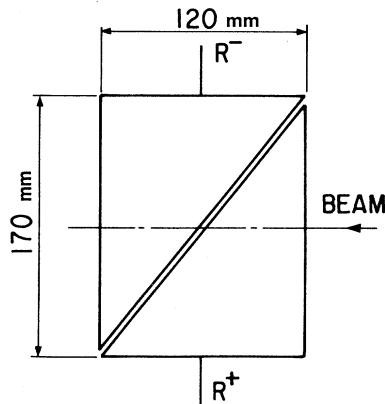


FIG. 3. Schematic view of the ion collector for beam-position measurements. The figure shows a top view of the ion collector.

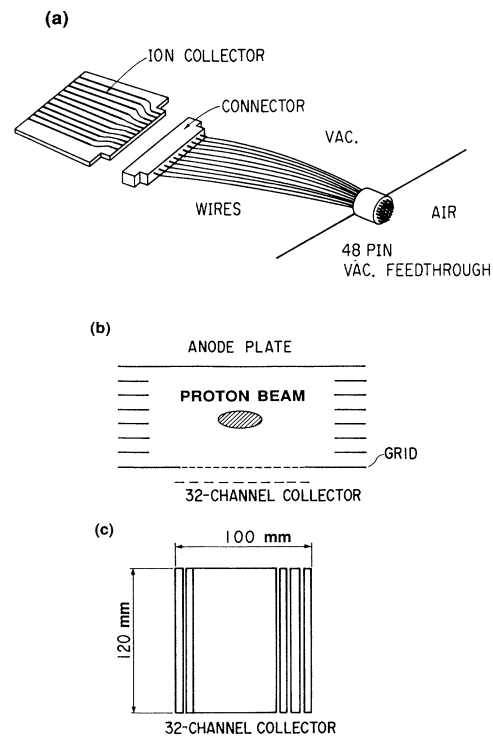


FIG. 4. Multichannel ion collector for beam-profile measurements. View (a) shows the arrangement of the ion collector and the connector. View (b) shows a horizontal cross-sectional view of the electrode structure. View (c) shows a vertical cross-section of the ion collector, which consists of 32 channels to allow the determination of a beam profile.

In summary, the clock pulses representing the instantaneous proton energy were fed to the readout time base of the transient recorder, and its output was graphically displayed. In this way, plots of the ionization cross section  $\sigma$  against proton energy  $T$  were displayed, as exemplified in Fig. 6. The data acquisition was highly

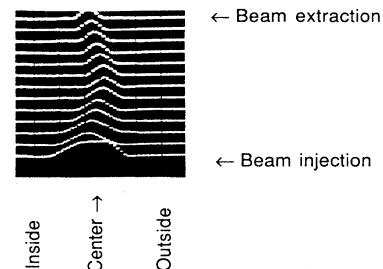


FIG. 5. Beam profiles observed with the ionization detector in the KEK-booster synchrotron. Each curve represents the beam profile, viz., the distribution of the lateral positions of protons at a fixed time. The bottom profile, observed immediately after the beam injection at 20 MeV, is broad. The profiles, observed at later and later times and shown upper and upper, become narrower as a result of acceleration. The peak position moves outward first, and inward eventually. The top profile, observed upon the beam extraction at 500 MeV, is narrow and its peak is located slightly inward of the center.

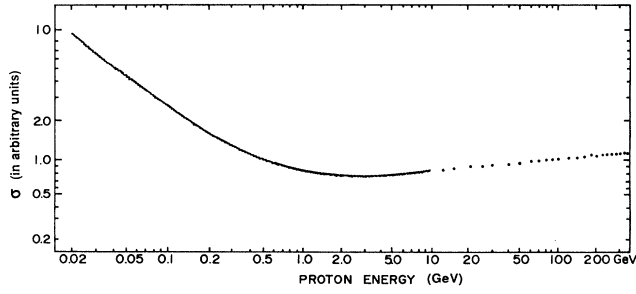


FIG. 6. An example of the plot of the ionization cross section  $\sigma$  of the residual gas as a function of the proton energy. The residual gas consisted mainly of air and contained a small amount of water vapor. The vertical axis represents the signal proportional to the ionization cross section. Data were taken with the KEK booster at 20–500 MeV, with the KEK main ring at 500 MeV to 12 GeV, and with the Fermilab main ring at 8–385 GeV.

efficient; in the KEK booster synchrotron, for example, it took only 25 ms to obtain  $\sigma$  for  $T$  between 20 and 500 MeV and less than a minute to display the data.

As a qualification, the data acquisition at the Fermilab main ring was carried out differently. The signals from the ionization detector and from the beam current monitor were fed into an oscilloscope, displayed as functions of time, and recorded photographically. Independently, the magnetic field in the main ring was also recorded similarly. Data were read from the resulting photographs. Consequently, the precision of the data is considerably inferior to that of the data taken at KEK, as seen from the scatter of data points above 10 GeV in Fig. 6.

#### E. Beam current monitor

As a beam current monitor, we used a feedbacktype current transformer consisting of a total of 3000 turns of coils. Around its core are 300 turns of a permalloy tape of width 30 mm and thickness 0.05 mm, as well as insulating glass tapes.

For achieving the reliability of the monitor signal, an applied voltage was kept constant within 0.1%, and the drift of an amplifier for signal detection within 0.5%. A transient recorder for data acquisition had a precision of about 0.5%. Consequently, the overall accuracy of the monitor signal was a few percent.

#### F. Beam intensities and energies

The KEK booster synchrotron accelerated about  $5 \times 10^{11}$  protons/pulse from 20 to 500 MeV. The KEK main ring accelerated about  $2 \times 10^{12}$  protons/pulse from 500 MeV to 12 GeV. Finally, the main ring at Fermilab accelerated  $2 \times 10^{13}$  protons/pulse from 8 to 385 GeV, during the period in which we conducted our measurements.

## IV. RESULTS OF MEASUREMENTS

### A. General remarks

With air as the target gas, we measured  $\sigma$  for  $T=20$ –500 MeV with the KEK booster synchrotron, for  $T=500$  MeV to 12 GeV with the KEK main ring, and for  $T=8$ –385 GeV with the Fermilab main ring. The data obtained with each of the three accelerators refer to nearly 1000 values of  $T$ . The three data sets were put on the same scale, so that they connect smoothly at 500 MeV and 8 GeV, at the transitions between accelerators. Results are shown in Fig. 6. We also took measurements on  $H_2$  and Ar with the use of the booster and the main ring at KEK.

As we discussed earlier, the values of  $T$  were determined from the clock pulses at an interval of  $10^{-5} T$ , while the deflecting magnetic field increased from  $9 \times 10^{-2}$  to 1.2 T. Thus, the energy determination is precise within 0.01%. Statistical uncertainties due to signal processing are estimated to be less than 1%, because we took precautions to avoid signal saturation in the transient recorders.

The cross-section data we report here remain relative. The experimental determination of absolute values would require calibration of the injected-gas pressure, as well as of the sensitivity of the ionization detector, both of which are left for future work.

### B. Data analysis following the Bethe theory

For a clear presentation of results and their interpretation, we will use some elements of the Bethe theory [8–12] to describe cross sections for ionization and excitation by protons at the kinetic energies used in the measurements. Moreover, the Bethe theory provides a way of putting the cross section values on the absolute scale.

For a particle of charge  $ze$  and speed  $v = \beta c$ , the Bethe theory gives the ionization cross section of the form [12–14]

$$\sigma = (8\pi z^2 a_0^2 R / mv^2)(M_i^2 x + C_i), \quad (2)$$

where  $a_0 = \hbar^2 / me^2 = 0.5292 \times 10^{-10}$  m is the Bohr radius,  $R = me^4 / (2\hbar^2) = 13.606$  eV is the Rydberg energy,  $M_i^2$  and  $C_i$  are dimensionless numbers that are properties of the target molecule (to be discussed later in full detail), and  $x$  is a variable solely dependent on  $\beta$ ,

$$x = \ln[\beta^2 / (1 - \beta^2)] - \beta^2. \quad (3)$$

The front factor has the dimension of area and may be alternatively written as

$$\begin{aligned} 8\pi z^2 a_0^2 R / mv^2 &= 4\pi z^2 a_0^2 (e^2 / \hbar c)^2 b^{-2} \\ &= 4\pi z^2 (\hbar / mc)^2 \beta^{-2}, \end{aligned} \quad (4)$$

where  $e^2 / \hbar c$  is the fine-structure constant, and  $\hbar / mc$  is the Compton wavelength. The constant  $4\pi (\hbar / mc)^2$  has the value  $1.874 \times 10^{-24}$  m<sup>2</sup>. According to the Bethe theory, the analytic form for the dependence of  $\sigma$  upon  $\beta$ , and hence upon the particle kinetic energy, is completely

predictable. Recognizing this, Fano [13] pointed out that it is most suitable to plot  $(mv^2/8\pi z^2 a_0^2 R)\sigma$  as a function of  $x$ . At sufficiently high particle speeds, the plot should approach a straight line.

Although data for the proton-impact ionization are scarce in our energy range, the cross sections at lower energies (up to several MeV) are found in the literature [1–3] for common gases; they indicate an approach to the straight-line behavior of the Fano plot. Note that Eq. (2) implies that, in the Bethe asymptotic region,  $\sigma$  depends on  $v$  but not explicitly on the particle mass; thus,  $\sigma$  for protons (or antiprotons) is the same as that for electrons (or positrons) having the same speeds. Protons in our energy range (20 MeV to 385 GeV) have the same speeds as electrons with energy from about 10 keV to 200 MeV. Ionization cross sections for electrons in this energy range (especially from 10 keV to several MeV) are available for common gases [14], and their energy dependence obeys Eq. (2). Consequently, we expect that our results should be represented closely by a straight line on the Fano plot; this is indeed the case, as is exemplified in Fig. 7.

The two coefficients  $M_i^2$  and  $C_i$  are characteristic of the molecule relevant to  $\sigma$ . The coefficient  $M_i^2$  is the total dipole matrix element squared, measured in  $a_0^2$ . Suppose that  $df/dE$  represents the density of the dipole oscillator strength per unit range of excitation energy  $E$  and that  $\eta_i(E)$  is the quantum yield for ionization of the molecular state at  $E > I$ , where  $I$  is the ionization threshold energy. Then, one may write [12]

$$M_i^2 = \int_I^\infty \eta_i(E) (R/E) (df/dE) dE. \quad (5)$$

The quantity  $M_i^2$  is related to the mean-squared radius of the valence shell, although it is not precisely equal to it. The values of  $M_i^2$  for many common molecules are known, at least at moderate accuracy, and their systematics are reasonably well understood [14–17].

The coefficient  $C_i$  depends on the dipole oscillator strength density  $df/dE$  as well as nondipole properties. In other words, it depends on the generalized oscillator strength for ionization as a function of both  $E$  and

momentum transfer  $\hbar K$ , as discussed fully by Inokuti [12]. The values of  $C_i$  for many molecules and its systematics have been discussed [14–17].

With the foregoing discussion as a background, we will consider the results of our measurements. Our  $\sigma$  values are relative; that is, they have been determined up to an unknown multiplicative factor (which depends on the molecule but *not* on the proton energy). Therefore, our  $\sigma$  values do not lead to values of the two coefficients  $M_i^2$  and  $C_i$ . Nevertheless, our  $\sigma$  values, when fitted to Eq. (2), lead to the ratio  $C_i/M_i^2$ . The values of this ratio can be compared with data in the literature.

Results for hydrogen and argon are summarized in Table I. The close agreement of our  $C_i/M_i^2$  values with those of Rieke and Prepejchal [14] gives us confidence not only in the correctness of our measurements but also in the interpretation of our results.

Rigorously speaking, comparison of our results with those of Rieke and Prepejchal [14] needs to be qualified. Our results are derived from measurements of the total charge (or the total number of electrons) produced by ionizing collisions, and the signal obtained is proportional to the *gross* ionization cross section, which scores single ionization with weight 1, double ionization with weight 2, triple ionization with weight 3, and so on, as fully discussed by de Heer and Inokuti [17]. In contrast, the results of Rieke and Prepejchal [14] are derived from measurements of the total number of ionizing collisions, and the signal obtained is proportional to the *counting* ionization cross section, which scores each ionizing collision with equal weight, regardless of the charge multiplicity of ions produced [17]. The distinction between the gross ionization cross section and the counting ionization cross section is barely significant for an atom or molecule containing a few electrons such as  $H_2$ , but is appreciable for an atom or molecule containing many electrons such as Ar, as fully discussed by Rudd *et al.* [1]. This issue certainly needs to be addressed when one discusses absolute cross-section values.

However, the value of  $C_i/M_i^2$  should be insensitive to the influence of multiple ionization for the following reason. As explained in Sec. 4.2 of Inokuti [12], one may define the coefficients  $M_{i,\tau}^2$  and  $C_{i,\tau}$  in the Bethe cross section for the  $\tau$ -fold ionization. Then, the coefficients  $M_{i,g}^2$  and  $C_{i,g}$  in the Bethe gross ionization cross section are given by

$$M_{i,g}^2 = \sum_\tau \tau M_{i,\tau}^2 \quad (6)$$

TABLE I. The ratio of the intercept to the slope of the Fano plot.

	Hydrogen	Argon
$C_i/M_i^2$		
Present measurements	11.6	8.86
Rieke and Prepejchal <sup>a</sup>	11.68	8.99
Rudd <i>et al.</i> <sup>b</sup>	12.1	10.3
$\ln(2mc^2/I)$ , derived from Ref. [20]	10.88	8.60

<sup>a</sup>Reference [14].

<sup>b</sup>Reference [2].

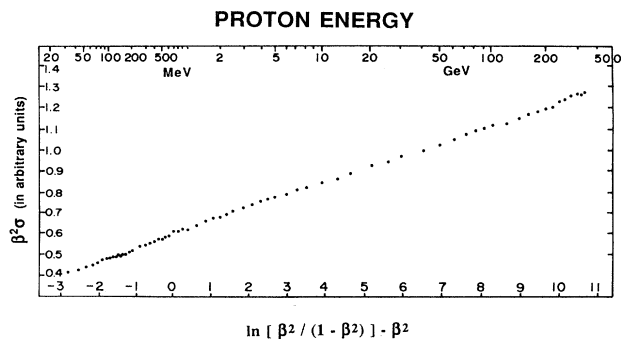


FIG. 7. An example of the Fano plot. Data are the same as in Fig. 6. The vertical axis represents  $\beta^2\sigma$  in arbitrary units. The horizontal axis at the bottom represents the variable  $x = \ln[\beta^2/(1-\beta^2)] - \beta^2$ , and the horizontal axis at the top, the bottom energy.

and

$$C_{i,g} = \sum_{\tau} \tau C_{i,\tau} . \quad (7)$$

The corresponding coefficients in the Bethe counting ionization cross section are given by

$$M_{i,c}^2 = \sum_{\tau} M_{i,\tau}^2 \quad (8)$$

and

$$C_{i,c} = \sum_{\tau} C_{i,\tau} . \quad (9)$$

Recall now the relation

$$C_n = M_n^2 (\ln c_n + 11.2268) , \quad (10)$$

viz., Eq. (4.27) of Inokuti [12], where the constant 11.2268 is the value of  $\ln(2mc^2/R)$ , and the suffix  $n$  specifies any outcome of an inelastic collision, e.g., the  $\tau$ -fold ionization. The quantity  $c_n$  is extensively discussed by Inokuti [12]. Studies of the numerical values of  $c_n$  for many atoms and molecules [14,18] indicate that  $c_n$  for various ionization processes are not far from unity; therefore,  $\ln c_n$  in Eq. (10) should be much smaller than 11.2268. The physical meaning of this statement is the dipole dominance, i.e., that the ionization cross section in general is predominantly determined by the strength of the dipole interactions represented by  $M_n^2$ . Then, it is reasonable to say that the ratio  $C_n/M_n^2$  should be roughly constant and close to 11, although it is hard to state the precision. Once we accept this argument, it is straightforward to conclude from Eqs. (6)–(9) that  $C_{i,g}/M_{i,g}^2$  should be roughly the same as  $C_{i,c}/M_{i,c}^2$ . In this sense, it is justified to compare the values of the ratio  $C_i/M_i^2$  derived from our measurements and those by Rieke and Prepejchal [14].

Table I also includes values derived from the gross ionization cross sections for protons in the MeV region, as given by Rudd *et al.* [2]. Table III of Rudd *et al.* [2] gives values of the coefficients  $A$  and  $B$  in their fitting equation, Eq. (33). Assuming that this equation tends to our Eq. (2), we may write

$$C_i/M_i^2 = B/A - \ln 4 - 11.2268 , \quad (11)$$

as seen from Eq. (4.56) of Inokuti [12]. The values thus derived are somewhat larger than the values from the present measurements and those of Rieke and Prepejchal [14]; perhaps the difference is attributable to departures from the Born approximation for which the fitting equation may not fully account.

### C. Additional remarks on data interpretation

It is useful to consider briefly the signal one would observe if one injected a gas at high pressure. At sufficiently high pressures, all the secondary electrons would be stopped by collisions with gas molecules in the collection volume of the ionization detector. Then, the signal  $s$  would be proportional to the total ionization rather than the primary ionization. Because the average energy required to produce an ion pair is nearly constant for sufficiently high energies of any charged particle [19],

the signal would be proportional to the mean energy loss of protons during their passage in the gas. So long as the relevant gas volume is sufficiently small to make the mean energy loss a small fraction of the proton kinetic energy, the signal would be proportional to the stopping power  $S$  of the gas for protons at that energy.

According to the Bethe theory [8–12,20],  $S$  is given by

$$S = 16\pi z^2 a_0^2 (R^2/mv^2) ZN [x + \ln(2mc^2/I)] , \quad (12)$$

where  $Z$  is the total number of electrons in a molecule,  $N$  is the number of molecules per unit volume of the gas, and the variable  $x$  is that defined by Eq. (3). The second term within the square brackets is a material constant, which is usually expressed in terms of the mean excitation energy  $I$  [20].

Compare Eq. (7) for  $S$  with Eq. (2) for  $\sigma$ , and note the following similarities and differences. The front factors are both proportional to  $\beta^{-2}$  and differ only by a constant factor. The remainders are both linear functions of  $x$ , but they have different coefficients. Thus, both  $S$  and  $\sigma$  should show straight lines on the Fano plot, although with different slopes and intercepts. From relative data (i.e., from the energy dependence of the signal apart from an overall factor), one can extract only the *ratio of the intercept to the slope*. This ratio is  $C_i/M_i^2$  for the ionization cross section  $\sigma$ ; it is  $\ln(2mc^2/I)$  for the stopping power. These two quantities are certainly different molecular properties, having different systematics. Thus, the knowledge about these quantities should allow us to determine whether the observed signal might be proportional to  $S$ .

To test this idea, we calculated the values of  $\ln(2mc^2/I)$  from the standard  $I$  values [20]. Results, included in Table I, are appreciably lower than the  $C_i/M_i^2$  values derived from the present measurements. Consequently, we conclude that the observed signal represents the ionization cross section rather than the stopping power.

At still higher pressures, we also expect the Fermi [21] density effect, which is usually discussed in reference to the stopping power [11]. The effect arises at relativistic speeds of any charged particle, because impact parameters relevant to energy losses are so large that many molecules are in the medium between the incident particle and a particular molecule that is excited or ionized. The electric polarization of the medium molecules causes reduction of energy losses. As a result, a straight line on the Fano plot for the stopping power will bend downward at extremely high speeds (i.e., at large  $x$ ) and will eventually turn to a plateau, as seen in measurements conducted at high pressures [22,23]. As expected at the lower pressure of  $10^{-5}$  Torr, we detected no such bending in the energy range of our measurements. The Fermi density effect at this pressure will become appreciable only at much higher proton energies.

### D. Experiments with an electron synchrotron

The Bethe theory predicts the same cross section for an electron and a proton at the same period. To verify this, we tried measurements with the electron synchrotron at

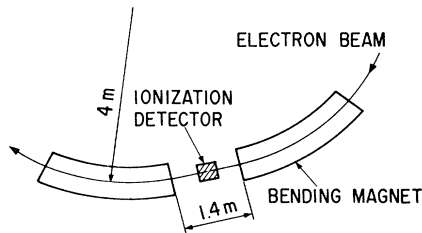


FIG. 8. Experimental setup at the electron synchrotron of the Institute for Nuclear Study, University of Tokyo.

the Institute for Nuclear Study, University of Tokyo, which accelerates electrons up to 1.3 GeV. We placed the ionization detector in the short, straight-line section of the vacuum duct as shown in Fig. 8. We did not specifically inject any gas, but there was residual gas pressure of about  $10^{-6}$  Torr.

Even when the ionization detector was positioned at the beam center (as indicated by an independent beam monitor), the signals  $R^+$  and  $R^-$  were different. The difference would suggest a beam displacement toward the outside by as much as 20 mm, which is totally inconsistent with the reading of the other beam monitor. The sum  $R^+ + R^-$ , which represents an apparent ionization cross section, gradually increased with increasing electron energy up to a few hundred MeV, indicating the familiar relativistic rise described by Eqs. (2) and (6). Beyond this electron energy, the signal grew extremely rapidly, as seen in Fig. 9.

The above observation is readily interpreted in terms of synchrotron radiation. The ultraviolet part, capable of photoionizing the residual gas, begins to be appreciable at electron energies of several hundred MeV in the synchrotron having the radius of 4 m. Moreover, the synchrotron radiation is emitted to the direction tangential to the beam, and, therefore, its intensity is greater outside the beam orbit. This explains the observation that  $R^+ > R^-$ . In conclusion, it was difficult to obtain an electron-impact ionization cross section from our experiments in the presence of synchrotron radiation. The same difficulty may arise for protons only at extremely high energies. Even at proton energies of tens of TeV, the intensity of the synchrotron radiation will be inappreciable, except at points of large orbital curvature.

## V. CONCLUDING REMARKS

We have measured the ionization cross section for protons over an unprecedented range of energies. The resulting energy dependence closely agrees with the prediction of the Bethe theory.

Two tasks are left for future work. First, it would be desirable to determine the absolute value of the ionization cross section from experiment. Results will permit closer comparison with other data and may shed new insights into some point of fundamental interest such as the multiple ionization.

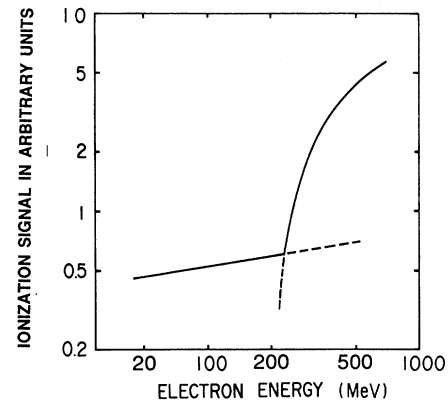


FIG. 9. An example of the ionization signal as a function of electron energy, observed with the electron synchrotron. The vertical axis shows the signal in arbitrary units. The part that gradually increases with the electron energy represents the ionization of the residual gas at  $10^{-6}$  Torr. The rapidly rising part at high electron energies represents ionization by synchrotron radiation.

Second, it would be even more desirable to extend the range of proton energies up to about 1 TeV, by the use of the Fermilab Tevatron. With the anticipated LHC, or other rings, storing protons in the TeV region, we would want to put many ionization monitors in the beam tube to detect any leak. At the same time, these monitors would enable us to measure ionization cross sections of gas molecules by using the techniques described here. Ionization measurements at extremely high energies might uncover some influence of the Fermi density effect or of synchrotron radiation effects.

*Note added in proof.* Ideas, similar to ours, of measuring ionization in a beam duct for beam and pressure monitoring have been discussed by O. Gröbner and P. Strubin [IEEE Trans. Nucl. Sci. NS-24, 1376 (1977)] and by A. Poncet [CERN MT/95-01 (ESH), LHC Note 316 (1995)].

## ACKNOWLEDGMENTS

We thank Professor Tetsuji Nishikawa and Professor Tohru Kamei for their support and encouragement throughout the present work. We are also indebted to Dr. Shigenori Hiramatsu, who provided the beam current monitor, to Dr. Ken-ichi Muto, who helped us with data processing and computer graphics, and to Mr. Zen'ei Igarashi, who built the circuitry for data acquisition and processing. Work at Fermi National Accelerator Laboratory was made possible by the permission and generous support by Dr. James E. Griffin, who installed a data-acquisition system in the main ring and made other crucial contributions. This work was supported in part by the U. S. Department of Energy, Office of Energy Research, Office of Health and Environmental Research, under Contract No. W-31-109-Eng-38.

- [1] M. E. Rudd, R. D. DuBois, L. H. Toburen, C. A. Ratcliffe, and T. V. Goffe, *Phys. Rev. A* **28**, 3244 (1983), and references therein.
- [2] M. E. Rudd, Y.-K. Kim, D. Madison, and J. W. Gallagher, *Rev. Mod. Phys.* **57**, 965 (1985).
- [3] E. W. McDaniel, M. E. Rudd, and J. B. Mitchell, *Atomic Collisions: Heavy Particle Projectiles* (Wiley, New York, 1993).
- [4] H. Ishimaru, K. Narushima, K. Kanazawa, Y. Suetsugu, D. Bintinger, H. Jöstlein, and D. Trobojevic, *J. Vac. Sci. Technol.* **6**, 1293 (1988).
- [5] W. H. DeLuca, *IEEE Trans. Nucl. Sci.* **NS-16**, 813 (1969).
- [6] H. Ishimaru, Z. Igarashi, S. Hiramatsu, and S. Shibata, in *Abstracts of Papers, VIth International Congress of Radiation Research, Tokyo, 1979*, edited by S. Okada, M. Imamura, T. Terasima, and H. Yamaguchi (Japanese Association for Radiation Research, Tokyo, 1979), p. 86.
- [7] H. Ishimaru, K. Muto, Z. Igarashi, S. Hiramatsu, S. Shibata, J. E. Griffin, and M. Inokuti, *Abstracts of Contributed Papers, XIth International Conference on the Physics of Electronic and Atomic Collisions, Kyoto, 1979*, edited by K. Takayanagi and N. Oda (North-Holland, Amsterdam, 1979), p. 640.
- [8] H. Bethe, *Ann. Phys. (Leipzig)* **5**, 325 (1930).
- [9] H. Bethe, *Z. Phys.* **76**, 293 (1932).
- [10] H. Bethe, in *Handbuch der Physik*, edited by H. Geiger and K. Scheel (Springer, Berlin, 1933), Vol. 24/1, p. 273.
- [11] U. Fano, *Ann. Rev. Nucl. Sci.* **13**, 1 (1963).
- [12] M. Inokuti, *Rev. Mod. Phys.* **43**, 297 (1971).
- [13] U. Fano, *Phys. Rev.* **95**, 1198 (1954).
- [14] F. F. Rieke and W. Prepejchal, *Phys. Rev. A* **6**, 1507 (1972).
- [15] M. Inokuti, R. P. Saxon, and J. L. Dehmer, *Int. J. Radiat. Phys. Chem.* **7**, 109 (1975).
- [16] M. Inokuti, J. L. Dehmer, T. Baer, and J. D. Hanson, *Phys. Rev. A* **23**, 95 (1981).
- [17] F. J. de Heer and M. Inokuti, in *Electron Impact Ionization*, edited by T. D. Märk and G. H. Dunn (Springer, Vienna, 1985), Chap. 7, p. 232.
- [18] M. Inokuti, J. L. Dehmer, T. Baer, and J. D. Hanson, *Phys. Rev. A* **23**, 95 (1981), Sec. V B.
- [19] International Commission on Radiation Units and Measurements, *Average Energy Required to Produce an Ion Pair*, ICRU Report No. 31 (International Commission on Radiation Units and Measurements, Washington, DC, 1979), and references therein.
- [20] International Commission on Radiation Units and Measurements, *Stopping Power for Electrons and Positrons*, ICRU Report No. 37 (International Commission on Radiation Units and Measurements, Bethesda, MD, 1984).
- [21] E. Fermi, *Phys. Rev.* **57**, 483 (1940).
- [22] A. H. Walenta, J. Fischer, H. Okuno, and C. L. Wang, *Nucl. Instrum. Methods* **161**, 45 (1979).
- [23] H. S. Virk, *Nucl. Phys. B* **72**, 393 (1974).